

Polarized consensus-based dynamics for optimization and sampling

Leon Bungert ^{*}

Tim Roith[†]

Philipp Wacker[‡]

June 12, 2025

Abstract

In this paper we propose polarized consensus-based dynamics in order to make consensus-based optimization (CBO) and sampling (CBS) applicable for objective functions with several global minima or distributions with many modes, respectively. For this, we “polarize” the dynamics with a localizing kernel and the resulting model can be viewed as a bounded confidence model for opinion formation in the presence of common objective. Instead of being attracted to a common weighted mean as in the original consensus-based methods, which prevents the detection of more than one minimum or mode, in our method every particle is attracted to a weighted mean which gives more weight to nearby particles. The resulting dynamics possess mean-field interpretations with Fokker–Planck equations that are structurally similar to the ones of original CBO and CBS, and we prove that the polarized CBS dynamics is unbiased in case of a Gaussian target. We also propose a computationally more efficient generalization which works with a predefined number of clusters and improves upon our polarized baseline method for high-dimensional optimization.

*“Ich überleg’ bei mir
Die nächsten Means dafür
Währenddessen ich noch rausch’.
Die Clusterzentren sind mir wohlbekannt,
Ich mein’, wir ham an Konsens auch.”*

loosely based on Hans Hölzel.

1 Introduction

Partially motivated by the success of machine learning methods, which involve the minimization of high-dimensional and strongly non-convex objectives, in recent years the interest in consensus-based methods which do not rely on first-order gradient information has constantly increased. Typically, zero-order optimization methods either construct a surrogate of the gradient and then perform a gradient-descent-type update [8] or use a swarm model [17, 21] where particles are attracted to the particle in the swarm which has the lowest objective value. Notably, the former approach can lead to problems for strongly non-convex objectives with many critical points. This issue is circumvented by swarm models, however, they typically do not allow for a mean-field description which makes their mathematical understanding difficult.

^{*}Hausdorff Center for Mathematics, University of Bonn, Endenicher Allee 62, Villa Maria, 53115 Bonn, Germany.
leon.bungert@hcm.uni-bonn.de

[†]Department of Mathematics, Friedrich-Alexander-Universität Erlangen-Nürnberg, Cauerstraße 11, 91058 Erlangen, Germany. tim.roith@fau.de

[‡]School of Mathematics and Statistics, University of Canterbury, Science Road, Ilam, Christchurch 8140, NZ. philipp.wacker@canterbury.ac.nz

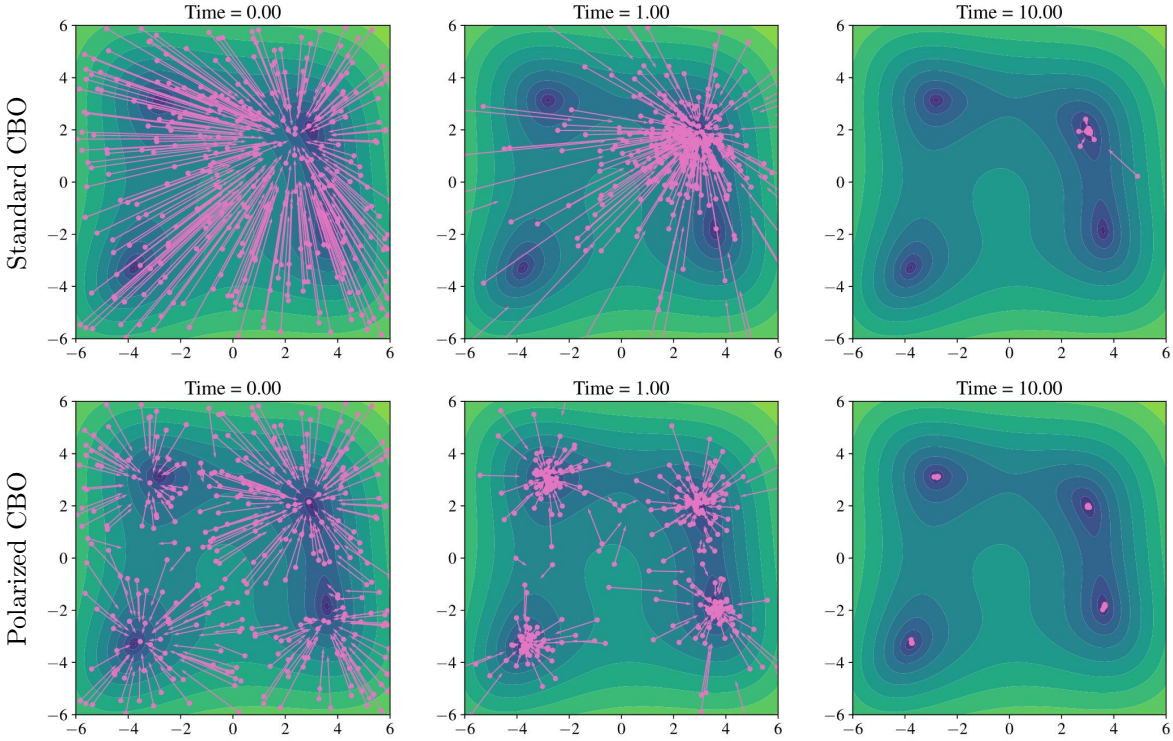


Figure 1: Dynamics of standard and the proposed polarized CBO for minimizing the Himmelblau function. The points mark particle locations, the arrows the drift field towards the weighted means.

In contrast, consensus-based methods aim to achieve consensus by letting particles $\{x^{(i)}\}_{i=1}^J$ explore the objective landscape while attracting them to the weighted average of their positions with respect to the Gibbs measure $\pi \propto \exp(-\beta V)$ of the objective function $V : \mathbb{R}^d \rightarrow \mathbb{R}$, where $\beta > 0$ is an inverse heat parameter. This method was first introduced in [19] as consensus-based optimization (CBO). As opposed to most other swarm methods CBO has a mean-field formulation involving a nonlinear Fokker–Planck equation. In [4] convergence to consensus of this equation was first proved, and [15] showed consensus formation of the discrete particle method. The key property for showing that the consensus is achieved close to the global minimum of the objective V is that $\exp(-\beta V)$ concentrates around the global minimizer of V as $\beta \rightarrow \infty$. More recently, [11] presented an improved convergence analysis which weakens some of the assumptions in [4] and directly proves convergence to a point close to the global minimum in a Wasserstein-2 distance.

Following up on the original formulation of CBO, numerous extensions were suggested. In [24] an additional drift term, modelling the time-average of the personal best of every particle, is proposed. In [7] an extension of the CBO method for constrained problems is suggested, and [6] adapted the method for high-dimensional problems from machine learning by introducing random batching and changing the noise model. In a different line of work, CBO methods on hypersurfaces were studied in [10] and applications to machine learning were investigated in [12]. In [22] CBO was enriched by ensemble-based gradient information which comes at low computational cost and can improve upon the baseline method. For an overview of recent developments we also refer to the review [23]. Consensus-based methods have also been transferred to sampling. The work [5] proposes a consensus-based sampling (CBS) method by changing the noise term in CBO to include a weighted sample covariance. This prevents a collapse of the ensemble to full consensus and under suitable assumptions the method was shown to converge to a Gaussian approximation of the distribution $\exp(-V)$.

While existing consensus-based methods have proven to work very well for non-convex objectives with many spurious local extreme points, they all suffer from the conceptual drawback that by definition they can at most compute one minimum, respectively one mode in the context of sampling. Therefore, the goal of this paper is to design consensus-based particle dynamics which support multiple consensus points, or in other words, polarization.

The central idea for the method which we are presenting in this paper is based on the following thought experiment: Assuming that two clusters of particles have formed, each one centered around a global minimum, we do not want to compute a shared weighted mean of their positions. This would pull one of the clusters into the other one. Therefore, we replace the weighted mean—being an integral component of current consensus-based methods—by a collection of localized means which additionally weigh particle positions by their proximity to the considered particle. The localization is achieved by a suitable kernel function. This then leads to polarized dynamics where multiple consensus points can be reached which allows for finding multiple global minima or multiple modes, respectively.

As we shall discuss in more detail later, our approach carries strong similarities to bounded confidence models of opinion formation, introduced in [9] but see also [13, 14, 16]. There agents only interact with each other if their opinions are sufficiently close, which in the end can lead to formation of multiple consensus points and is referred to as polarization of opinions in [16].

Main contributions The focus of this paper is the development of the novel polarized consensus-based dynamics and an extensive numerical evaluation of the method. The mathematical models we propose come with a lot of new theoretical questions, as well, which will be the subject of future investigations. The main contributions and structure of this paper can be summarized as follows:

- Section 2.1: We propose a novel polarized computation of weighted means for CBO methods.
- Section 2.2: We propose an algorithmic variant which uses a predetermined number of cluster points to compute weighted means.
- Section 2.3: We propose a novel polarized computation of weighted covariances for the CBS method and prove that it is unbiased for Gaussian targets.
- Section 3: We conduct extensive numerical and statistical evaluations of our polarized optimization method, showing that it can find multiple global minima in low and high dimensional optimization problems and can even improve upon standard CBO for the detection of one minimum. We also test our polarized CBS method for sampling from mixtures of Gaussian and a non-Gaussian distribution where it exhibits better performance than standard CBS.

2 Models

In this section we describe in detail how standard consensus-based models work and how we generalize them with our polarized approach. For this, we let $V : \mathbb{R}^d \rightarrow [0, \infty)$ be a (possibly non-convex) objective function and $\beta > 0$ an inverse heat parameter.

2.1 Polarized consensus-based optimization

Given a measure $\rho \in \mathcal{M}(\mathbb{R}^d)$, for standard CBO one defines a weighted mean as

$$\mathbf{m}_\beta[\rho] := \frac{\int y \exp(-\beta V(y)) d\rho(y)}{\int \exp(-\beta V(y)) d\rho(y)}. \quad (2.1)$$

Here and in the rest of the paper all integrals will be over \mathbb{R}^d . The consensus-based optimization method from [19] then amounts to solving the following system of stochastic differential equations

(SDEs) for particles $\{x^{(i)}\}_{i=1,\dots,J}$:

$$dx^{(i)} = -(x^{(i)} - \mathbf{m}_\beta[\rho]) dt + \sigma \left| x^{(i)} - \mathbf{m}_\beta[\rho] \right| dW^{(i)}, \quad \rho := \frac{1}{J} \sum_{i=1}^J \delta_{x^{(i)}}, \quad (2.2)$$

where $\{W^{(i)}\}_{i=1}^J$ denote independent Brownian motions and $\sigma \geq 0$ determines the strength of the randomness in the model. The Fokker–Planck equation associated to (2.2) is the following PDE

$$\partial_t \rho_t(x) = \operatorname{div} \left(\rho_t(x)(x - \mathbf{m}_\beta[\rho_t]) \right) + \frac{\sigma^2}{2} \Delta \left(\rho_t(x) |x - \mathbf{m}_\beta[\rho]|^2 \right). \quad (2.3)$$

As explained above, this dynamical system forces particles to collapse to consensus, meaning that under certain conditions on V the empirical measures $\rho(t)$ converge to $\delta_{\hat{x}}$ as $t \rightarrow \infty$, where for $\beta \rightarrow \infty$ the consensus-point \hat{x} converges to the global minimizer of V , see [4, 11].

We now explain our polarized modification of CBO for optimizing objective functions with multiple global minima. Given a measure $\rho \in \mathcal{M}(\mathbb{R}^d)$ and a kernel function $\mathbf{k} : \mathbb{R}^d \times \mathbb{R}^d \rightarrow [0, \infty)$ we define the weighted mean

$$\mathbf{m}_{\beta,\mathbf{k}}[\rho](x) := \frac{\int \mathbf{k}(x, y) y \exp(-\beta V(y)) d\rho(y)}{\int \mathbf{k}(x, y) \exp(-\beta V(y)) d\rho(y)}, \quad x \in \mathbb{R}^d. \quad (2.4)$$

The corresponding polarized optimization dynamics take the form

$$dx^{(i)} = -(x^{(i)} - \mathbf{m}_{\beta,\mathbf{k}}[\rho](x^{(i)})) dt + \sigma \left| x^{(i)} - \mathbf{m}_{\beta,\mathbf{k}}[\rho](x^{(i)}) \right| dW^{(i)}, \quad \rho := \frac{1}{J} \sum_{i=1}^J \delta_{x^{(i)}}, \quad (2.5)$$

and the Fokker–Planck equation associated to (2.5) is the following PDE

$$\partial_t \rho_t(x) = \operatorname{div} \left(\rho_t(x)(x - \mathbf{m}_{\beta,\mathbf{k}}[\rho_t](x)) \right) + \frac{\sigma^2}{2} \Delta \left(\rho_t(x) |x - \mathbf{m}_{\beta,\mathbf{k}}[\rho_t](x)|^2 \right). \quad (2.6)$$

Note that the idea of letting the dynamics of particle $x^{(i)}$ mainly depend on spatially close particles, as modelled through the kernel \mathbf{k} , has strong similarities to bounded confidence models of opinion dynamics introduced in [9]. In these models, typically there is no objective function to be minimized and the kernel is of the form $\mathbf{k}(x, y) := 1_{|x-y| \leq \kappa}(x, y)$, where $\kappa > 0$ is a so-called confidence level. The simplest such dynamics then take the form

$$\frac{dx^{(i)}}{dt} = - \left(x^{(i)} - \frac{1}{N(x^{(i)})} \sum_{j=1}^J 1_{|x^{(i)} - x^{(j)}| \leq \kappa} x^{(j)} \right), \quad (2.7)$$

where $N(x^{(i)}) := \#\{1 \leq j \leq J : |x^{(i)} - x^{(j)}| \leq \kappa\}$ denotes the numbers of points which are not farther than κ away from $x^{(i)}$. Notably, (2.7) coincides with (2.5) for the special case of $\mathbf{k}(x, y) := 1_{|x-y| \leq \kappa}(x, y)$, a constant objective $V \equiv \text{const}$, and $\sigma = 0$. More generally, dynamics of the form (2.5) and (2.7) can be viewed as processes on co-evolving networks or graphs where the weights between different particles $x^{(i)}$ and $x^{(j)}$ depend on the kernel \mathbf{k} and the loss function V . We refer to [2, 3] for a unified description and the study of mean-field equations for general processes of this form.

In the following, we would like to discuss two important special cases of our model: If one chooses the kernel $\mathbf{k}(x, y) = 1$ for all $x, y \in \mathbb{R}^d$, then (2.4) to (2.6) simply reduce to the standard CBO setup (2.1) to (2.3). Hence, our method is a generalization of CBO. On the other hand, if one chooses the Gaussian kernel $\mathbf{k}(x, y) := \exp\left(-\frac{|x-y|^2}{2\kappa^2}\right)$, then the weighted mean $\mathbf{m}_{\beta,\mathbf{k}}[\rho](x)$ can be rewritten as

$$\mathbf{m}_{\beta,\mathbf{k}}[\rho](x) := \frac{\int y \exp\left(-\beta V(y) - \frac{|x-y|^2}{2\kappa^2}\right) d\rho(y)}{\int \exp\left(-\beta V(y) - \frac{|x-y|^2}{2\kappa^2}\right) d\rho(y)}. \quad (2.8)$$

In this case our method can be regarded as standard CBO applied to a spatially varying quadratic regularization of the objective function $y \mapsto V_x(y)$, defined as

$$V_x(y) := V(y) + \frac{1}{2\kappa^2\beta} |x - y|^2.$$

Note that the central difference between the standard and our method is that the weighted mean (2.4) depends on the particle position x and is not same for all particles.

Especially for high-dimensional problems it was shown in [6] that the performance of CBO can be significantly improved when using a coordinate-wise noise model. To be precise they suggest the following replacement in (2.5)

$$\left| x^{(i)} - \mathbf{m}_{\beta,k}[\rho](x^{(i)}) \right| dW^{(i)} \longrightarrow \sum_{n=1}^d \vec{e}_n \left(x^{(i)} - \mathbf{m}_{\beta,k}[\rho](x^{(i)}) \right)_n dW_n^{(i)}, \quad (2.9)$$

where \vec{e}_n denotes the n -th unit vector in \mathbb{R}^d . This changes the Laplacian term in the corresponding Fokker–Planck equation (2.6) to

$$\Delta(\rho_t(x) |x - \mathbf{m}_{\beta,k}[\rho_t](x)|) \longrightarrow \sum_{n=1}^d \partial_{nn}^2 \left(\rho_t(x)(x - \mathbf{m}_{\beta,k}[\rho_t](x))_n \right).$$

For computing an approximate solution of the stochastic CBO dynamics with either of the two discussed noise models, we employ a standard Euler–Maruyama scheme which we sum up in Algorithm 1. There the function **ComputeMean** determines the precise variant of CBO that is being used. In Algorithm 2 we specify this function for the proposed polarized CBO which reduces to standard CBO for a constant kernel $k \equiv 1$. In the next section we will discuss an algorithmic variant (see Algorithm 3) of the mean computation (2.4) which is computationally more efficient and exhibits empirical advantages in high dimensions.

Algorithm 1: General consensus-based optimization

Input: Time step size $dt > 0$, initial particles $\{x^{(j)}\}_{j=1}^J$, diffusion parameter $\sigma \geq 0$, noise model M

for $i = 1, \dots, J$ **do**

- $\mathbf{m}^{(i)} \leftarrow \mathbf{ComputeMean}$
- if** $M = \text{Standard noise}$ **then**

 - $\xi \sim \mathcal{N}(0, dt \cdot I_{d \times d})$
 - $n^{(i)} \leftarrow |x^{(i)} - \mathbf{m}^{(i)}| \xi$

- end**
- if** $M = \text{Coordinate noise}$ **then**

 - $\xi \sim \mathcal{N}(0, dt \cdot I_{d \times d})$
 - $n^{(i)} \leftarrow \sum_{n=1}^d e_n (x^{(i)} - \mathbf{m}^{(i)})_n \xi_n$

- end**
- $x^{(i)} \leftarrow x^{(i)} - dt(x^{(i)} - \mathbf{m}^{(i)}) + \sigma n^{(i)}$

end

2.2 Cluster-based model

In this section we propose an algorithmic alternative to the weighted mean, defined in (2.4) with the motivation of making the computation of the weighted means computationally more efficient and to

Algorithm 2: ComputeMean for polarized CBO

Input: particle $x^{(i)}$, particle swarm $\{x^{(j)}\}_{j=1}^J$, kernel \mathbf{k} , objective V , inverse temperature $\beta > 0$

Output: $\mathbf{m}^{(i)} \leftarrow \frac{\sum_{j=1}^J x^{(j)} \mathbf{k}(x^{(i)}, x^{(j)}) \exp(-\beta V(x^{(j)}))}{\sum_{j=1}^J \mathbf{k}(x^{(i)}, x^{(j)}) \exp(-\beta V(x^{(j)}))}$

also encourage polarizing effects between the different means. Given particles $x^{(i)}$ for $i = 1, \dots, J$, standard CBO uses one weighted mean whereas our polarized version uses J many weighted means.

As an alternative model we consider cluster means $\mathbf{c}^{(j)}$ for $j = 1, \dots, J_c$, where $J_c \leq J$. We encode the probability that the particle $x^{(i)}$ belongs to the cluster mean $\mathbf{c}^{(j)}$ with $p_{ij} > 0$. In this setting we perform the following update for each $j = 1, \dots, J_c$,

$$p_i^{\max} := \max_{j=1, \dots, J_c} p_{ij} \quad \text{for } i = 1, \dots, J, \quad (2.10a)$$

$$r_{ij} := \left(\frac{p_{ij}}{p_i^{\max}} \right)^\alpha \quad \text{for } i = 1, \dots, J, \quad (2.10b)$$

$$\tilde{p}_{ij} := r_{ij} \mathbf{k}(x^{(i)}, \mathbf{c}^{(j)}). \quad (2.10c)$$

Here, $\alpha \geq 0$ is a discounting coefficient. The interpretation of the above scheme is as follows: If the particle $x^{(i)}$ identifies the cluster center $\mathbf{c}^{(j)}$ as ‘‘belonging to it the most’’, then $r_{ij} = 1$ and the probability that $x^{(i)}$ indeed belongs to $\mathbf{c}^{(j)}$ is only determined by the spatial proximity, encoded through $\mathbf{k}(x^{(i)}, \mathbf{c}^{(j)})$. If, however, it ‘‘feels more dedicated’’ to another cluster mean $\mathbf{c}^{(k)}$ (different from $\mathbf{c}^{(j)}$), then $p_{ij} < p_{ik}$ and thus $r_{ij} < 1$. This results in a correction of the particle-cluster correspondence, strengthening particle i is bound to cluster j , favoring strengthening of established connections. The exponent $\alpha \geq 0$ determines the strength of this additional polarization incentive, with larger $\alpha \geq 0$ leading to greater polarization.

The new values of the probabilities p_{ij} are then obtained by renormalization over j , i.e.,

$$p_{ij} := \frac{\tilde{p}_{ij}}{\sum_{j=1}^{J_c} \tilde{p}_{ij}} \quad (2.11)$$

and the clusters means are then updated via

$$\mathbf{c}^{(j)} := \frac{\sum_{i=1}^J x^{(i)} p_{ij} \exp(-\beta V(x^{(i)}))}{\sum_{i=1}^J p_{ij} \exp(-\beta V(x^{(i)}))}. \quad (2.12)$$

In order to obtain the individual mean for each particle (like in the polarized CBO scheme) we simply compute

$$\mathbf{m}^{(i)} := \sum_{j=1}^{J_c} p_{ij} \mathbf{c}^{(j)}. \quad (2.13)$$

We summarize the cluster-based mean computations in Algorithm 3, which can be used in place of Algorithm 2 in the CBO scheme Algorithm 1.

Note that for $\alpha = \infty$ we have that

$$r_{ij} := \begin{cases} 1, & \text{if } j \in \arg \max_{j=1, \dots, J_c} p_{ij}, \\ 0, & \text{else,} \end{cases}$$

meaning that the only probability which survive are the one for the likeliest cluster centers. Another interesting special case arises when choosing the Gaussian kernel $\mathbf{k}(x, y) := \exp\left(-\frac{|x-y|^2}{2\kappa^2}\right)$. In this

Algorithm 3: ComputeMean for cluster-based method

Input: particle $x^{(i)}$, particle swarm $\{x^{(j)}\}_{j=1}^J$, cluster centers $\{\mathbf{c}^{(j)}\}_{j=1}^{J_c}$, probabilities $\{p_{ij}\}_{j=1}^{J_c}$, discounting coefficient $\alpha \geq 0$, kernel \mathbf{k} , objective V , inverse temperature $\beta > 0$

$p_i^{\max} \leftarrow \max_{j=1, \dots, N_c} p_{ij}$ ▷ Compute probability of likeliest cluster

for $j = 1, \dots, J_c$ **do**
 | $r_{ij} \leftarrow \left(\frac{p_{ij}}{p_i^{\max}}\right)^\alpha$
 | $\tilde{p}_{ij} \leftarrow r_{ij} \mathbf{k}(x^{(i)}, \mathbf{c}^{(j)})$ ▷ Discount probabilities for other clusters
end

for $j = 1, \dots, J_c$ **do**
 | $p_{ij} \leftarrow \frac{\tilde{p}_{ij}}{\sum_{j=1}^{J_c} \tilde{p}_{ij}}$ ▷ Normalize probabilities
end

for $j = 1, \dots, J_c$ **do**
 | $\mathbf{c}^{(j)} \leftarrow \frac{\sum_{i=1}^J x^{(i)} p_{ij} \exp(-\beta V(x^{(i)}))}{\sum_{i=1}^J p_{ij} \exp(-\beta V(x^{(i)}))}$ ▷ Update cluster centers
end

Output: $m_i \leftarrow \sum_{j=1}^{J_c} p_{ij} \mathbf{c}^{(j)}$

case one gets that

$$p_{ij} := \frac{\exp\left(-\frac{1}{2\kappa^2} |x^{(i)} - \mathbf{c}^{(j)}|^2 + \log r_{ij}\right)}{\sum_{j=1}^{J_c} \exp\left(-\frac{1}{2\kappa^2} |x^{(i)} - \mathbf{c}^{(j)}|^2 + \log r_{ij}\right)}$$

$$\rightarrow \begin{cases} 1 & \text{if } |x^{(i)} - \mathbf{c}^{(j)}| \leq |x^{(i')} - \mathbf{c}^{(j')}| \quad \forall i' = 1, \dots, J, j' = 1, \dots, J_c, \\ 0 & \text{else,} \end{cases} \quad \text{as } \kappa \rightarrow 0.$$

So for very small values of κ a hard assignment of the points $x^{(i)}$ to the clusters $\mathbf{c}^{(j)}$ based on spatial proximity is performed which is reminiscent of the k-means algorithm.

It is important to initialize all quantities correctly in order to obtain a meaningful algorithm. If one naively initializes $p_{ij} := \frac{1}{J_c}$ for all $i = 1, \dots, J$ and computes initial cluster centers via (2.12), then $\mathbf{c}^{(j)} = \frac{\sum_{i=1}^J x^{(i)} \exp(-\beta V(x^{(i)}))}{\sum_{i=1}^J \exp(-\beta V(x^{(i)}))}$ equals the standard CBO weighted mean for all j . Correspondingly, the probability updates (2.10) and (2.11) will leave p_{ij} untouched. In this case the method reduces precisely to standard CBO. Therefore, we initialize the probabilities randomly by drawing $\tilde{p}_{ij} \sim \text{Unif}(0, 1)$ and normalizing with (2.11). Then we compute initial cluster means using (2.12).

Let us also mention that the complexity of CBO where means are computed with Algorithm 3 is order $O(J \cdot J_c)$ which is significantly smaller than $O(J^2)$ which is the complexity of CBO with the baseline polarized mean computation from Algorithm 2. This is due to the fact that the cluster-based method models consensus and polarization of individuals with respect to existing opinionated groups, with the cluster center as a surrogate for these groups, whereas the polarized CBO approach tracks all particles' interactions with each other.

Last, we demonstrate how to obtain a SDE and mean-field interpretation of Algorithm 3, where

for conciseness we restrict ourselves to the case $\alpha = 0$. In this case (2.11) and (2.12) reduce to

$$p_{ij} \leftarrow \frac{\mathbf{k}(x^{(i)}, \mathbf{c}^{(j)})}{\sum_{j=1}^{J_c} \mathbf{k}(x^{(i)}, \mathbf{c}^{(j)})}, \quad \mathbf{c}^{(j)} \leftarrow \frac{\sum_{i=1}^J x^{(i)} \mathbf{k}(x^{(i)}, \mathbf{c}^{(j)}) \exp(-\beta V(x^{(i)}))}{\sum_{i=1}^J \mathbf{k}(x^{(i)}, \mathbf{c}^{(j)}) \exp(-\beta V(x^{(i)}))}.$$

This allows us to express the cluster-based mean computation with $\alpha = 0$ as the coupled system:

$$dx^{(i)} = -(x^{(i)} - \mathbf{m}^{(i)}) dt + \sigma |x^{(i)} - \mathbf{m}^{(i)}| dW^{(i)}, \quad (2.14a)$$

$$\mathbf{m}^{(i)} = \frac{\sum_{j=1}^{J_c} \mathbf{k}(x^{(i)}, \mathbf{c}^{(j)}) \mathbf{c}^{(j)}}{\sum_{j=1}^{J_c} \mathbf{k}(x^{(i)}, \mathbf{c}^{(j)})}, \quad (2.14b)$$

$$\mathbf{c}^{(j)} = \frac{\int x \mathbf{k}(x, \mathbf{c}^{(j)}) \exp(-\beta V(x)) d\rho_t(x)}{\int \mathbf{k}(x, \mathbf{c}^{(j)}) \exp(-\beta V(x)) d\rho_t(x)}, \quad (2.14c)$$

$$\rho_t := \frac{1}{N} \sum_{i=1}^J \delta_{x^{(i)}}. \quad (2.14d)$$

Note that Algorithm 3 approximates the fixed point equation for $\mathbf{c}^{(j)}$ with one iteration of the fixed point map. The corresponding mean-field system is readily obtained as:

$$\partial_t \rho_t(x) = \operatorname{div}(\rho_t(x)(x - \mathbf{m}[\rho_t](x))) + \frac{\sigma^2}{2} \Delta \left(\rho_t(x) |x - \mathbf{m}[\rho_t](x)|^2 \right), \quad (2.15a)$$

$$\mathbf{m}[\rho_t](x) = \frac{\sum_{j=1}^{J_c} \mathbf{k}(x, \mathbf{c}^{(j)}) \mathbf{c}^{(j)}}{\sum_{j=1}^{J_c} \mathbf{k}(x, \mathbf{c}^{(j)})}, \quad (2.15b)$$

$$\mathbf{c}^{(j)} = \frac{\int x \mathbf{k}(x, \mathbf{c}^{(j)}) \exp(-\beta V(x)) d\rho_t(x)}{\int \mathbf{k}(x, \mathbf{c}^{(j)}) \exp(-\beta V(x)) d\rho_t(x)}. \quad (2.15c)$$

We expect that similarly one can derive a SDE and mean-field interpretation of the model with $\alpha > 0$ but we do not endeavour this here.

2.3 Polarized consensus-based sampling

The last model variant that we consider here is an application to sampling. In [5] a sampling version of CBO was proposed and termed consensus-based sampling (CBS). Defining a weighted covariance matrix as

$$\mathbf{C}_\beta[\rho] := \frac{\int (y - \mathbf{m}_\beta[\rho]) \otimes (y - \mathbf{m}_\beta[\rho]) \exp(-\beta V(y)) d\rho(y)}{\int \exp(-\beta V(y)) d\rho(y)}. \quad (2.16)$$

CBS aims to sample from the measure $\exp(-V)$ and by solving the following system of SDEs:

$$dx^{(i)} = -(x^{(i)} - \mathbf{m}_\beta[\rho]) dt + \sqrt{2\lambda^{-1} \mathbf{C}_\beta[\rho]} dW^{(i)}, \quad \rho := \frac{1}{J} \sum_{i=1}^J \delta_{x^{(i)}}. \quad (2.17)$$

Here the parameter λ interpolates between an optimization method ($\lambda = 1$) and a sampling method ($\lambda = (1 + \beta)^{-1}$). For the latter scaling of λ a collapse of ρ is avoided and ρ samples from $\exp(-V)$ if this measure is Gaussian. The Fokker-Planck equation associated with (2.17) is given by

$$\partial_t \rho_t(x) = \operatorname{div} \left(\rho_t(x)(x - \mathbf{m}_\beta[\rho_t]) \right) + \lambda^{-1} \operatorname{div} \left(\mathbf{C}_\beta[\rho_t] \nabla \rho_t(x) \right). \quad (2.18)$$

We can polarize CBS by using the mean from (2.4) to define a weighted variance, as follows:

$$C_{\beta,k}[\rho](x) := \frac{\int k(x,y)(y - m_{\beta,k}[\rho](x)) \otimes (y - m_{\beta,k}[\rho](x)) \exp(-\beta V(y)) d\rho(y)}{\int k(x,y) \exp(-\beta V(y)) d\rho(y)}, \quad x \in \mathbb{R}^d. \quad (2.19)$$

The corresponding CBS dynamics are then

$$dx^{(i)} = -(x^{(i)} - m_{\beta,k}[\rho](x^{(i)})) dt + \sqrt{2\lambda^{-1}C_{\beta,k}[\rho](x^{(i)})} dW^{(i)}, \quad \rho := \frac{1}{J} \sum_{i=1}^J \delta_{x^{(i)}}, \quad (2.20)$$

and the associated Fokker–Planck equation is

$$\partial_t \rho_t(x) = \operatorname{div}(\rho_t(x)(x - m_{\beta,k}[\rho_t](x))) + \lambda^{-1} \operatorname{div}(C_{\beta,k}[\rho_t](x) \nabla \rho_t(x)). \quad (2.21)$$

Perhaps a little unexpectedly we can prove that, just as the Fokker–Planck equation of CBS (2.18), for Gaussian kernels of arbitrary width our version (2.21) leaves Gaussians measures invariant, which is an important consistency property.

Proposition 2.1. *The polarized CBS dynamics in sampling mode with a Gaussian kernel leaves a Gaussian target measure invariant.*

More precisely, let $k(x,y) := \exp(-\frac{1}{2}(x-y)^T \Sigma_1^{-1}(x-y))$ for a symmetric and positive definite covariance matrix $\Sigma_1 \in \mathbb{R}^{d \times d}$, and let

$$V(y) := \frac{1}{2}(x-m)^T \Sigma_2^{-1}(x-m)$$

for some $m \in \mathbb{R}^d$ and a symmetric and positive definite covariance matrix $\Sigma \in \mathbb{R}^{d \times d}$. Then ρ^* defined as

$$\rho^*(x) := \exp(-V(x))$$

is a stationary solution of the Fokker–Planck equation (2.21) for any $\beta > 0$ and for $\lambda = (1+\beta)^{-1}$.

Proof. We use a following formula for the product of two Gaussians, which can be found, for instance, in [18], to obtain

$$\begin{aligned} k(x,y) \exp(-(1+\beta)V(y)) &= \exp\left(-\frac{1}{2}(x-y)^T \Sigma_1^{-1}(x-y)\right) \exp\left(-\frac{1+\beta}{2}(x-m)^T \Sigma_2^{-1}(x-m)\right) \\ &= c_x \exp\left(-\frac{1}{2}(y-m_x)^T \Sigma_3(y-m_x)\right), \end{aligned}$$

where $c_x > 0$ is a normalization constant and

$$\begin{aligned} \Sigma_3 &:= (\Sigma_1^{-1} + (1+\beta)\Sigma_2^{-1})^{-1}, \\ m_x &:= \Sigma_3(\Sigma_1^{-1}x + (1+\beta)\Sigma_2^{-1}m). \end{aligned}$$

Using this we obtain

$$\begin{aligned} \int k(x,y) \exp(-\beta V(y)) d\rho^*(y) &= \int k(x,y) \exp(-(1+\beta)V(y)) dy \\ &= c_x \int \exp\left(-\frac{1}{2}(y-m_x)^T \Sigma_3(y-m_x)\right) dy \\ &= c_x (2\pi)^{\frac{d}{2}} \det(\Sigma_3)^{\frac{1}{2}}. \end{aligned}$$

Similarly, we obtain

$$\begin{aligned} \int y \mathbf{k}(x, y) \exp(-V(y)) d\rho^*(y) &= c_x \int y \exp\left(-\frac{1}{2}(y - m_x)^T \Sigma_3 (y - m_x)\right) dy \\ &= c_x (2\pi)^{\frac{d}{2}} \det(\Sigma_3)^{\frac{1}{2}} m_x. \end{aligned}$$

Combining the two we obtain

$$\mathbf{m}_{\beta, \mathbf{k}}[\rho^*](x) = m_x.$$

Similarly, we can compute the weighted covariance as

$$\begin{aligned} \mathbf{C}_{\beta, \mathbf{k}}[\rho^*](x) &= \frac{\int (x - \mathbf{m}_{\beta, \mathbf{k}}[\rho^*](x)) \otimes (x - \mathbf{m}_{\beta, \mathbf{k}}[\rho^*](x)) \mathbf{k}(x, y) \exp(-\beta V(y)) d\rho^*(y)}{\int \mathbf{k}(x, y) \exp(-V(y)) d\rho^*(y)} \\ &= \frac{c_x \int (x - m_x) \otimes (x - m_x) c_x \exp\left(-\frac{1}{2}(y - m_x)^T \Sigma_3 (y - m_x)\right) dy}{c_x (2\pi)^{\frac{d}{2}} \det(\Sigma_3)^{\frac{1}{2}}} = \Sigma_3. \end{aligned}$$

Hence, we get for $\lambda = (1 + \beta)^{-1}$:

$$\begin{aligned} &\rho^*(x)(x - \mathbf{m}_{\beta, \mathbf{k}}[\rho^*](x)) + \lambda^{-1} \mathbf{C}_{\beta, \mathbf{k}}[\rho^*](x) \nabla \rho^*(x) \\ &= \rho^*(x)(x - m_x) + (1 + \beta) \Sigma_3 \nabla \rho^*(x) \\ &= \rho^*(x)(x - m_x) - (1 + \beta) \Sigma_3 \nabla V(x) \rho^*(x) \\ &= \rho^*(x) \left((x - m_x) - (1 + \beta) \Sigma_3 \Sigma_2^{-1}(x - m) \right) \end{aligned}$$

Now we use the definition of $m_x = \Sigma_3(\Sigma_1^{-1}x + (1 + \beta)\Sigma_2^{-1}m)$ to obtain

$$\begin{aligned} &x - m_x - (1 + \beta) \Sigma_3 \Sigma_2^{-1}(x - m) \\ &= x - \Sigma_3(\Sigma_1^{-1}x + (1 + \beta)\Sigma_2^{-1}m) - (1 + \beta) \Sigma_3 \Sigma_2^{-1}(x - m) \\ &= x - \Sigma_3(\Sigma_1^{-1} + (1 + \beta)\Sigma_2^{-1})x = 0, \end{aligned}$$

using that $\Sigma_3 = (\Sigma_1^{-1} + (1 + \beta)\Sigma_2^{-1})^{-1}$. This proves that ρ^* is a stationary solution of the Fokker–Planck equation (2.21). \square

2.4 Some remarks on the analysis

In this section we will make some remarks on the analysis of the Fokker–Planck equation (2.6) for polarized CBO which we repeat here for convenience:

$$\partial_t \rho_t(x) = \operatorname{div} \left(\rho_t(x)(x - \mathbf{m}_{\beta, \mathbf{k}}[\rho_t](x)) \right) + \frac{\sigma^2}{2} \Delta \left(\rho_t(x) |x - \mathbf{m}_{\beta, \mathbf{k}}[\rho](x)|^2 \right).$$

Weak solutions of this equation are continuous curves of probability measures $t \mapsto \rho_t$ such that

$$\frac{d}{dt} \int \phi(x) d\rho_t(x) = - \int \nabla \phi(x) \cdot (x - \mathbf{m}_{\beta, \mathbf{k}}[\rho_t](x)) d\rho_t(x) + \frac{\sigma^2}{2} \int \Delta \phi(x) |x - \mathbf{m}_{\beta, \mathbf{k}}[\rho_t](x)|^2 d\rho_t(x)$$

holds true for all smooth and compactly supported test functions $\phi \in C_c^\infty(\mathbb{R}^d)$.

Using the Leray–Schauder fixed point theorem, existence proofs for this equation without a kernel, i.e., $\mathbf{k}(x, y) = 1$, were given in [4, 11] under mild assumptions on the objective V and for initial distributions with finite fourth-order moment. Taking into account that

$$\mathbf{k}(x, y) \exp(-\beta V(y)) = \exp\left(-\beta \left(V(y) - \frac{1}{\beta} \log \mathbf{k}(x, y)\right)\right)$$

we expect that under reasonable Lipschitz-like assumptions on the logarithm of the kernel these arguments translate to our case, but we leave this for future work. The biggest challenge is that for standard CBO $t \mapsto \mathbf{m}_\beta[\rho_t]$ is a continuous curve in \mathbb{R}^d , whereas $t \mapsto \mathbf{m}_{\beta,k}[\rho_t](\cdot)$ is not. Rather, it is a curve in a space of vector fields. This requires more sophisticated compactness arguments than the one made in [4, 11].

Besides existence, in the literature there exist two different approaches to proving formation of consensus around the global minimizer of V for the Fokker–Planck equation (2.3) associated to standard CBO. The first one was presented in [4] and constitutes a two-step approach. First, they prove that the non-weighted standard variance

$$V(\rho_t) := \int |x - E(\rho_t)|^2 \, d\rho_t(x), \quad \text{where } E(\rho_t) := \int y \, d\rho_t(y),$$

decreases to zero along solutions ρ_t of (2.3). This obviously implies that ρ_t converges to a Dirac measure $\delta_{\tilde{x}}$ concentrated on some point $\tilde{x} \in \mathbb{R}^d$. Second, the Laplace principle is invoked in order to conclude that \tilde{x} lies close to the global minimizer of V if β is chosen sufficiently large. This analytical approach uses heavily that the weighted mean $\mathbf{m}_\beta[\rho_t]$ for CBO *does not* depend on the spatial variable x which is a linearity property that our weighted mean $\mathbf{m}_{\beta,k}[\rho_t](x)$ does not enjoy. Furthermore, by design our method does in general not converge to a single Dirac mass and hence it's classical variance does not converge to zero.

A different approach is presented in [11] where the authors propose a more unified strategy. For this they fix a point $\hat{x} \in \mathbb{R}^d$ (which later will be the global minimizer of V) and define the variance-type function

$$V[\rho_t] := \frac{1}{2} \int |x - \hat{x}|^2 \, d\rho_t(x). \quad (2.22)$$

The authors note that $V[\rho_t] = \frac{1}{2} \mathcal{W}_2^2(\rho_t, \delta_{\hat{x}})$ and so convergence of the variance implies convergence of ρ_t to $\delta_{\hat{x}}$ in the Wasserstein-2 distance. They derive a differential inequality for $V[\rho_t]$ which in combination with the Laplace principle allows them to show some kind of semi-convergence behavior, i.e., for every $\varepsilon > 0$ there exists $\beta > 0$ such that $V[\rho_t]$ decreases exponentially fast until it hits the threshold $V[\rho_t] \leq \varepsilon$.

When it comes to generalizing this approach to our setting there are two main obstacles. First, in the case of several global minimizers $\{\hat{x}_i : 1 \leq i \leq N\}$ the Wasserstein-2 distance between ρ_t and the empirical measure $\frac{1}{N} \sum_{i=1}^N \delta_{\hat{x}_i}$ does not equal $\frac{1}{N} \sum_{i=1}^N \int |x - \hat{x}_i|^2 \, d\rho_t(x)$. Indeed, the latter quantity is a very bad upper bound for the desired Wasserstein-2 distance since it is bounded from below by a positive number.

Albeit, we can still prove the following generalization of [11, Lemma 18], where we use the notation

$$\|\mathbf{m}_{\beta,k}[\rho_t](\cdot) - \hat{x}\|_{L^2(\rho_t)}^2 := \int |\mathbf{m}_{\beta,k}[\rho_t](x) - \hat{x}|^2 \, d\rho_t(x).$$

Lemma 2.2. *Let $\hat{x} \in \mathbb{R}^d$ be arbitrary and let $t \mapsto \rho_t$ be a weak solution of (2.6). Then it holds that*

$$\begin{aligned} \frac{d}{dt} V[\rho_t] &\leq -(2 - d\sigma^2) V[\rho_t] + \sqrt{2}(1 + d\sigma^2) \sqrt{V[\rho_t]} \|\mathbf{m}_{\beta,k}[\rho_t](\cdot) - \hat{x}\|_{L^2(\rho_t)} \\ &\quad + \frac{d\sigma^2}{2} \|\mathbf{m}_{\beta,k}[\rho_t](\cdot) - \hat{x}\|_{L^2(\rho_t)}^2. \end{aligned}$$

Proof. Using that ρ_t is a weak solution of (2.6) we get

$$\begin{aligned}
\frac{d}{dt}V[\rho_t] &= -\frac{1}{2} \int \nabla |x - \hat{x}|^2 \cdot (x - \mathbf{m}_{\beta,k}[\rho_t](x)) d\rho_t(x) \\
&\quad + \frac{\sigma^2}{2} \frac{1}{2} \int \Delta |x - \hat{x}|^2 |\mathbf{m}_{\beta,k}[\rho_t](x) - x|^2 d\rho_t(x) \\
&= - \int (x - \hat{x}) \cdot (x - \mathbf{m}_{\beta,k}[\rho_t](x)) d\rho_t(x) \\
&\quad + \frac{d\sigma^2}{2} \int |\mathbf{m}_{\beta,k}[\rho_t](x) - x|^2 d\rho_t(x) = T_1 + T_2.
\end{aligned}$$

We estimate both terms separately. Using the Cauchy–Schwarz inequality we can bound T_1 as follows:

$$\begin{aligned}
T_1 &= -2V[\rho_t] + \int (x - \hat{x}) \cdot (\mathbf{m}_{\beta,k}[\rho_t](x) - \hat{x}) d\rho_t(x) \\
&\leq -2V[\rho_t] + \sqrt{\int |x - \hat{x}|^2 d\rho_t(x)} \sqrt{\int |\mathbf{m}_{\beta,k}[\rho_t](x) - \hat{x}|^2 d\rho_t(x)} \\
&\leq -2V[\rho_t] + \sqrt{2V[\rho_t]} \|\mathbf{m}_{\beta,k}[\rho_t](\cdot) - \hat{x}\|_{L^2(\rho_t)}.
\end{aligned}$$

Next, we bound T_2 by expanding the square and using Cauchy–Schwarz:

$$\begin{aligned}
T_2 &= \frac{d\sigma^2}{2} \int |\mathbf{m}_{\beta,k}[\rho_t](x) - x|^2 d\rho_t(x) \\
&= \frac{d\sigma^2}{2} \int \left(|x - \hat{x}|^2 - 2(x - \hat{x}) \cdot (\mathbf{m}_{\beta,k}[\rho_t] - \hat{x}) + |\mathbf{m}_{\beta,k}[\rho_t] - \hat{x}|^2 \right) d\rho_t(x) \\
&\leq d\sigma^2 \left(V[\rho_t] + \int |x - \hat{x}| |\mathbf{m}_{\beta,k}[\rho_t] - \hat{x}| d\rho_t(x) + \frac{1}{2} \|\mathbf{m}_{\beta,k}[\rho_t](\cdot) - \hat{x}\|_{L^2(\rho_t)}^2 \right) \\
&\leq d\sigma^2 \left(V[\rho_t] + \sqrt{2V[\rho_t]} \|\mathbf{m}_{\beta,k}[\rho_t](\cdot) - \hat{x}\|_{L^2(\rho_t)} + \frac{1}{2} \|\mathbf{m}_{\beta,k}[\rho_t](\cdot) - \hat{x}\|_{L^2(\rho_t)}^2 \right).
\end{aligned}$$

Combining both estimates completes the proof. \square

The fundamental issue which prevents a straightforward adaption of the arguments in [11], using Lemma 2.2, is that the term $\|\mathbf{m}_{\beta,k}[\rho_t](\cdot) - \hat{x}\|_{L^2(\rho_t)}$ is in general not small, even if \hat{x} is the global minimizer of V and β is very large. This is due to the presence of the localizing kernel in the definition of the weighted mean $\mathbf{m}_{\beta,k}[\rho_t](\cdot)$ in (2.4). Also, we expect and designed our method to cluster particles around similarly good minimizers, not just around the global optimum. Similarly to [11] one would have to make strict assumptions on the initial distribution and the kernel to prove that sufficiently much mass is concentrated around the minimizer and deduce convergence.

3 Numerical examples

In this section we evaluate the numerical performance of the proposed algorithms. In all our experiments we chose a time step parameter of $dt = 0.01$. The code to reproduce all numerical experiments is available on GitHub¹.

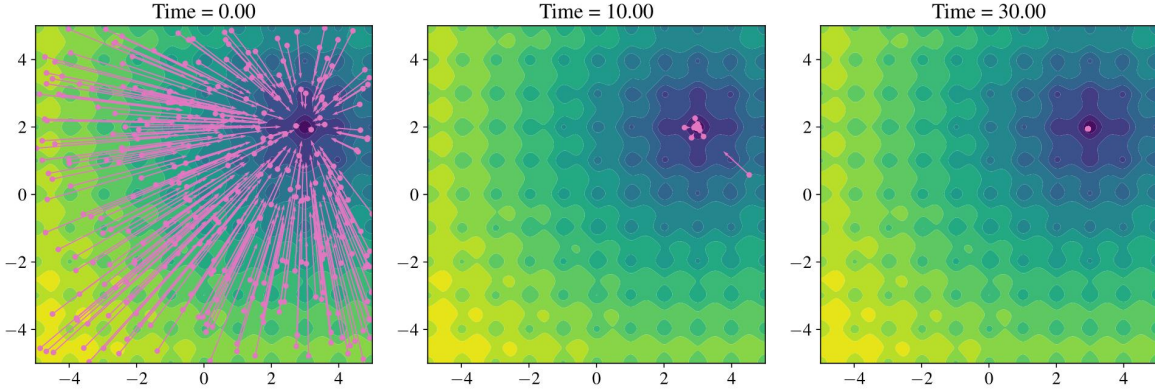


Figure 2: Dynamics of standard CBO for minimizing the Ackley function. The points mark particle locations, the arrows the drift field towards the shared weighted mean.

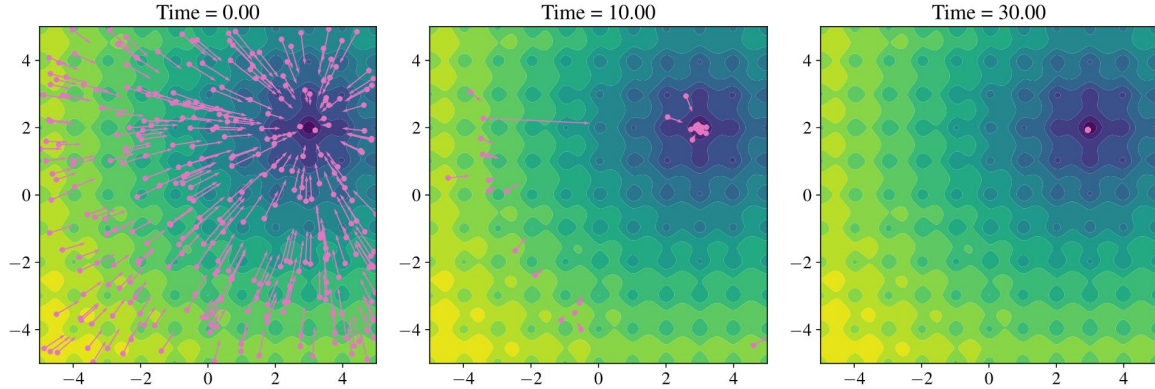


Figure 3: Dynamics of the proposed polarized CBO for minimizing the Ackley function. The points mark particle locations, the arrows the drift field towards the individual weighted means.

3.1 Unimodal Ackley function

In the first example we perform a consistency check for our method for finding the unique global minimum of the Ackley function [1], defined as

$$A(x) := -20 \exp\left(-\frac{0.2}{\sqrt{d}} |x|\right) - \exp\left(\frac{1}{d} \sum_{n=1}^d \cos(2\pi x_n)\right) + e + 20. \quad (3.1)$$

This function has a global minimum at $0 \in \mathbb{R}^d$ with $A(0) = 0$ and in this experiment we choose $d = 2$ and minimize the shifted version $V(x) := A(x - (3, 2))$ which has its global minimum at $(3, 2) \in \mathbb{R}^2$. We compare the dynamics of standard CBO with our proposed polarized variant at three different time points in Figures 2 and 3. We use the Gaussian kernel $k(x, y) := \exp\left(-\frac{|x-y|^2}{2\kappa^2}\right)$ with standard deviation $\kappa = \infty$ for standard CBO and $\kappa = 1$ for polarized CBO. Furthermore, we choose $\beta = 1$. In this easy situation with a unique global minimum we observe that both standard and polarized CBO find the global minimum and do not get stuck in local minima. Notably, the polarized variant converges slightly slower than standard CBO which is due to the localization effect of the kernel with a relatively small standard deviation.

¹<https://github.com/TimRoith/PolarCBO>

3.2 Multimodal Rastrigin function

In this example we evaluate different choices of kernel functions for minimizing a Rastrigin-type function with three global minima. The original Rastrigin function [20] on \mathbb{R}^d is defined as

$$R(x) := 10d + \sum_{n=1}^d (x_n^2 - 10 \cos(2\pi x_n)) \quad (3.2)$$

and has a global minimum at $x = 0$ with $U(0) = 0$. In this experiment we choose $d = 2$ and minimize the product

$$V(x) = \frac{1}{8} R(x) R(x - (3, 2)) R(x + (1, 3.5))$$

which has three global minima. Note that this function is very non-convex and at the same time extremely flat around its minima, see Figure 4 for a surface plot.

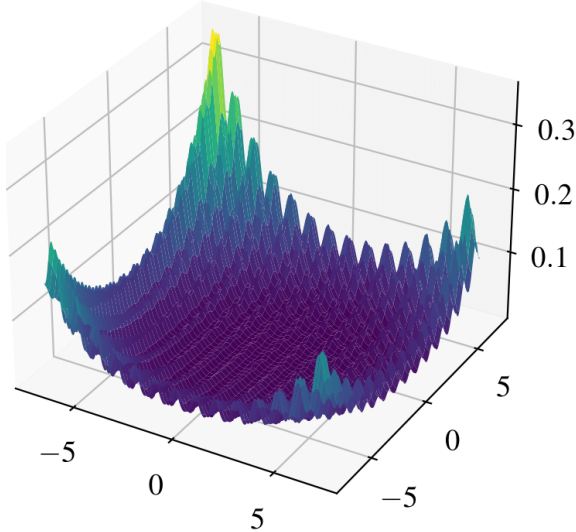


Figure 4: A variant of the Rastrigin function with three global minima

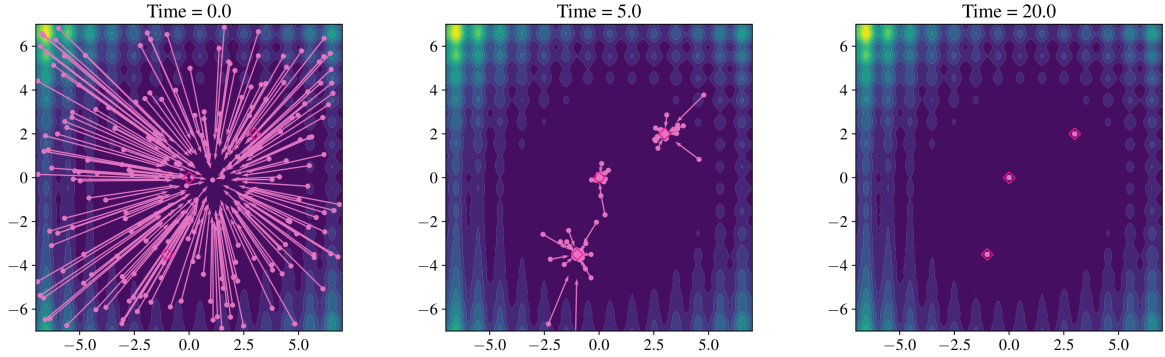
We consider the three different kernels

$$k(x, y) = \exp\left(-\frac{|x - y|^2}{2\kappa^2}\right) \quad \text{Gaussian kernel,} \quad (3.3)$$

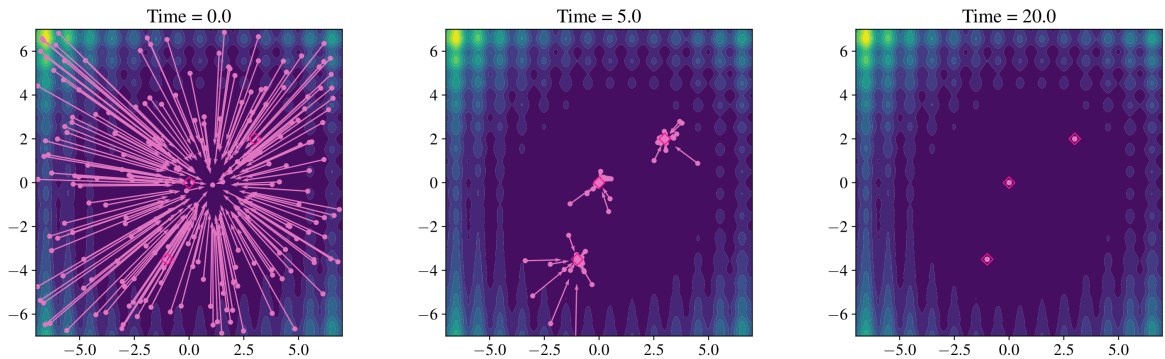
$$k(x, y) = \exp\left(-\frac{|x - y|}{\kappa}\right) \quad \text{Laplace kernel,} \quad (3.4)$$

$$k(x, y) = 1_{|x - y| \leq \kappa}(x, y) \quad \text{bounded confidence kernel,} \quad (3.5)$$

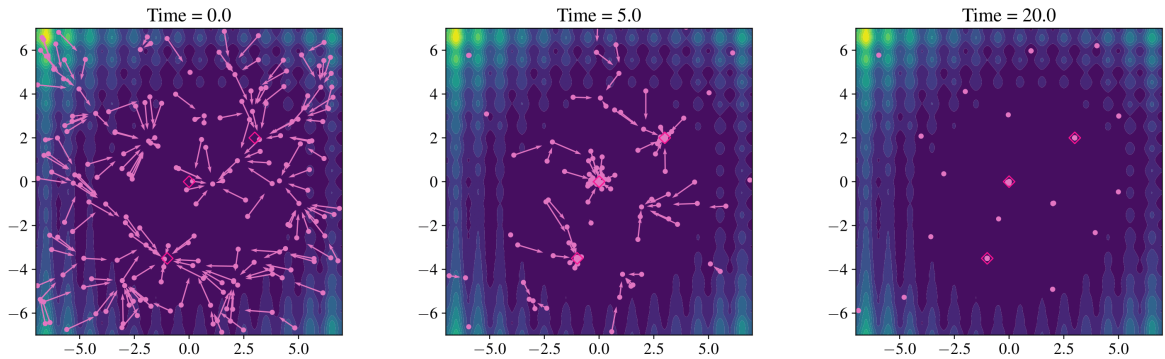
and the corresponding results of our method are depicted in Figure 5. Again, we choose $\beta = 1$. The kernel parameters κ were chosen sufficiently small for the methods to detect all three minima, which are marked with blue diamonds. While the Gaussian and the Laplace kernel work similarly well—note however that the Laplace kernel needs a much smaller value of κ than the Gaussian—the bounded confidence kernel (cf. the discussion in Section 2.1) works suboptimally for the task of minimization. While it manages to detect all three minima a lot of particles get stuck in suboptimal consensus points which can be explained by the fact that the kernel has compact support.



(a) Gaussian kernel with $\kappa = 0.5$



(b) Laplace kernel with $\kappa = 0.05$.



(c) Bounded confidence kernel with $\kappa = 2$.

Figure 5: Dynamics of polarized CBO with different kernels for minimizing a Rastrigin-type function with three global minima, marked by red diamonds. For all kernels all minima were detected. Gaussian and Laplace kernel work especially well, whereas the bounded confidence kernel generates too many consensus points due to its compact support.

Polarized	# minima	J = 25			J = 50			J = 100			J = 200		
		≥ 1	≥ 2	≥ 3	≥ 1	≥ 2	≥ 3	≥ 1	≥ 2	≥ 3	≥ 1	≥ 2	≥ 3
	$\kappa = 0.1$	33%	7%	0%	86%	59%	24%	100%	96%	67%	100%	100%	97%
	$\kappa = 0.5$	100%	62%	5%	100%	78%	18%	100%	93%	41%	100%	100%	84%
	$\kappa = 1$	100%	5%	0%	100%	12%	0%	100%	14%	0%	100%	24%	0%
	CBO	100%	0%	0%	100%	0%	0%	100%	0%	0%	100%	0%	0%

Table 1: Performance of polarized CBO for minimizing the multimodal Ackley function with $d = 2$ and three global minima: Averaging over 100 independent runs of 1,000 iterations we plot how many percent of the succeeded in detecting *at least* 1, 2, or 3 of the minima. Note that, by definition, standard CBO ($\kappa = \infty$) can detect *at most one* minimum.

3.3 Multimodal Ackley function

We proceed with quantitative evaluations of our method for a multimodal version of the Ackley function (3.1), defined as

$$V(x) := \prod_{i=1}^N A(x - z_i),$$

where $\{z_i \in \mathbb{R}^d : i = 1, \dots, N\}$ are points which constitute the global minimizers of V , and U is the standard Ackley function defined in (3.1). In Table 1 we plot how many of the three minima in dimension $d = 2$ were detected by the proposed polarized CBO method with a Gaussian kernel and different values of the standard deviation κ . That means, we show the percentage of runs that detected at least 1, 2, or 3 minima. Here, we employed the standard noise model as specified in (2.5) with $\sigma = 1.0$ and $\beta = 1.0$. For completeness we also include results for standard CBO (i.e., $\kappa = \infty$) which by definition can detect at most one minimum.

We say that a method detects a minimum if at convergence there exists a weighted mean $\mathbf{m}_{\beta,k}[\rho](x)$ which is closer than 0.25 in the infinity norm to the minimum. For standard CBO where $\mathbf{m}_{\beta,k}[\rho](x) = \mathbf{m}_\beta[\rho]$ for all x this coincides with the definition of success in [5, 19]. For our experiments we employ $N = 3$ different minima $z_1, z_2, z_3 \in \mathbb{R}^d$ with

$$(z_1)_i := \begin{cases} -2 & \text{if } i \bmod 2 = 0, \\ 1 & \text{else,} \end{cases} \quad (z_2)_i := \begin{cases} 2 & \text{if } i \bmod 2 = 0, \\ -1 & \text{else,} \end{cases} \quad (z_3)_i := \begin{cases} -1 & \text{if } i \bmod 2 = 0, \\ -3 & \text{else} \end{cases}$$

for $i = 1, \dots, d$.

While polarized CBO works very well in the two-dimensional example, Table 2 shows that in dimension $d = 10$, it fails to detect more than one minimum. However, the cluster method from 3 exhibits significantly improved behavior and manages to detect all three minima frequently. Here, we employed the coordinate-wise noise model from (2.9) with $\sigma = 7.5$. Additionally we employed a simple scheduling for the parameter β , where we start with $\beta = 30$ and increase it in each step via

$$\beta \leftarrow 1.01 \cdot \beta$$

up to a limit of $\beta_{\max} = 10^7$. Here, one could potentially employ more sophisticated approaches as proposed in [5]. For the cluster-based methods we chose $\alpha = 5.0$ in Algorithm 3.

Even for $\kappa = \infty$, where the kernel has no influence anymore, the method works very well. Note that this case does not correspond to standard CBO. Furthermore, Table 2 shows that our polarized method can outperform standard CBO at finding at least one minimum, albeit at the cost of higher complexity.

We also test the cluster method in $d = 30$ dimensions and the results can be found in Table 3. We observe that it is harder to find multiple minima, however for $J = 1600$ the method finds at least two minima in over 50% of the runs for $\kappa \geq 1$. For smaller particle numbers the algorithm performs better for $\kappa \leq 1$, although the percentage of runs, where multiple minima are found is very low.

		$J = 50$			$J = 100$			$J = 200$			$J = 400$		
		≥ 1	≥ 2	≥ 3	≥ 1	≥ 2	≥ 3	≥ 1	≥ 2	≥ 3	≥ 1	≥ 2	≥ 3
Polarized Cluster	$\kappa = 0.001$	5%	0%	0%	18%	0%	0%	26%	0%	0%	63%	1%	0%
	$\kappa = 0.01$	26%	0%	0%	56%	0%	0%	80%	1%	0%	79%	3%	0%
	$\kappa = 0.1$	36%	0%	0%	68%	0%	0%	73%	0%	0%	75%	0%	0%
	CBO	32%	0%	0%	55%	0%	0%	74%	0%	0%	72%	0%	0%
	$\kappa = 10^{-7}$	26%	2%	0%	75%	26%	2%	98%	59%	13%	100%	89%	28%
	$\kappa = 0.1$	11%	1%	0%	68%	13%	0%	98%	77%	19%	100%	96%	39%
Cluster	$\kappa = \infty$	6%	0%	0%	65%	11%	0%	98%	73%	15%	100%	92%	41%

Table 2: Performance of polarized and cluster CBO for minimizing the multimodal Ackley function with $d = 10$ and ceteris paribus. The first method is slightly better than CBO but fails to detect more than one minimum in most cases. The cluster variant works well for a wide range of parameters κ and manages to detect all minima when using 200 or more particles. Note that $\kappa = \infty$ *does not* correspond to CBO for this method.

		$J = 200$			$J = 400$			$J = 800$			$J = 1600$		
		≥ 1	≥ 2	≥ 3	≥ 1	≥ 2	≥ 3	≥ 1	≥ 2	≥ 3	≥ 1	≥ 2	≥ 3
Cluster	$\kappa = 0.01$	15%	0%	0%	61%	5%	0%	92%	28%	1%	99%	45%	1%
	$\kappa = 0.1$	9%	0%	0%	59%	6%	0%	94%	34%	2%	98%	49%	2%
	$\kappa = 1$	4%	0%	0%	57%	5%	0%	88%	40%	0%	97%	57%	4%
	$\kappa = 10$	5%	0%	0%	58%	7%	0%	89%	35%	1%	98%	58%	1%
	$\kappa = 100$	4%	0%	0%	59%	7%	0%	89%	32%	0%	98%	57%	2%
	$\kappa = \infty$	5%	0%	0%	58%	6%	0%	88%	33%	0%	98%	54%	2%

Table 3: Performance of cluster CBO for minimizing the multimodal Ackley function with $d = 30$ and ceteris paribus.

3.4 Multimodal sampling

In this section we consider the task of sampling from a bimodal mixture of Gaussians.

$$\exp(-V(x)) := \exp\left(-(x_1 - a_1)^2 - \frac{(x_2 - a_2)^2}{0.2}\right) + \frac{1}{2} \exp\left(-\frac{(x_1 - b_1)^2}{8} - \frac{(x_2 - b_2)^2}{0.5}\right),$$

where the tuples $a = (a_1, a_2)$ and $b = (b_1, b_2)$ determine the centers of the clusters. In Figure 6 we plot the result of standard CBS and our polarized variant using Gaussian kernels with three different standard deviations $\kappa \in \{0.4, 0.6, 0.8\}$. For both methods we choose $\beta = 1$. Note that, at least for convex potentials V with bounded Hessian, standard CBS is known to exhibit a Gaussian steady state. Being designed as a method for unimodal sampling, there is not much hope CBS can work in this multimodal situation. Still we include CBS results for comparison.

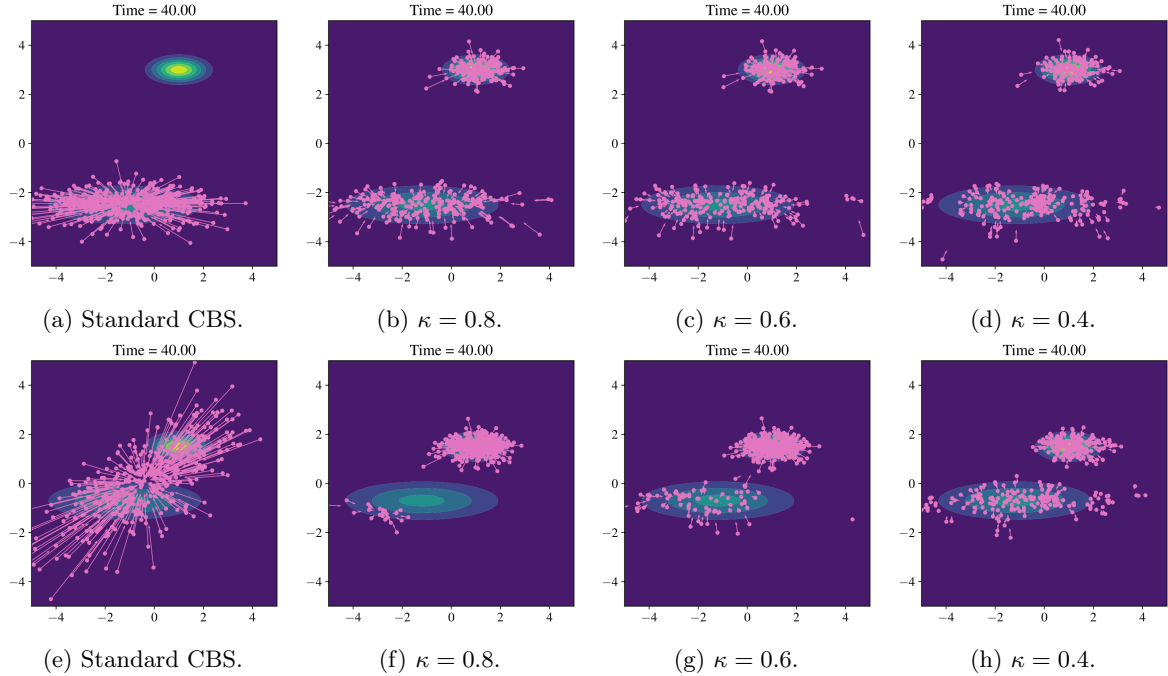


Figure 6: Dynamics of standard CBS and our polarized version, sampling from a mixture of Gaussians (top row: far apart, bottom row: closer together). The points mark particle locations, the arrows the drift field towards the weighted mean(s).

In contrast, our polarized modification of CBS manages to isolate the two modes. Note that in Proposition 2.1 we proved that polarized CBS with a Gaussian kernel is unbiased when the target measure is a Gaussian. We do not expect this to be true for target measures which are a mixture of Gaussians. Still, our results in the first row of Figure 6 show that, if the two Gaussians are sufficiently far apart, our method (second to fourth column) seems close to being unbiased. Standard CBS (left column) can, by design, find at most one mode and here it successfully detects the lower Gaussian. Note that we use the same number of particles for both algorithms, namely $J = 400$, which is why the bottom mode for CBS looks more densely sampled.

The situation is different when the two modes are closer together, as shown in the bottom row of Figure 6. Here, standard CBS fails to detect even one mode whereas our polarized version does achieve that. However, as expected in this multimodal situation the result is not a perfect sample but appears to be biased. Furthermore, if the clusters are close, the sensitivity with respect to the choice of the kernel width κ is larger and κ has to be chosen sufficiently small in order to generate enough samples for the lower cluster.

3.5 Non-Gaussian sampling

Our final experiment deals with sampling from a non-Gaussian distribution. Again, we use $\beta = 1$. According to the theoretical analysis in [5] standard CBS is not expected to correctly sample from such a distribution but rather from a Gaussian approximation. While we do not claim that our polarized method generates an exact sample, our result in Figure 7 show that polarized CBS approximates the non-Gaussian distribution much better than standard CBS. This is due to the fact that the weighted means, indicated as orange crosses, do not collapse to a single point but concentrate in the region of high probability mass.

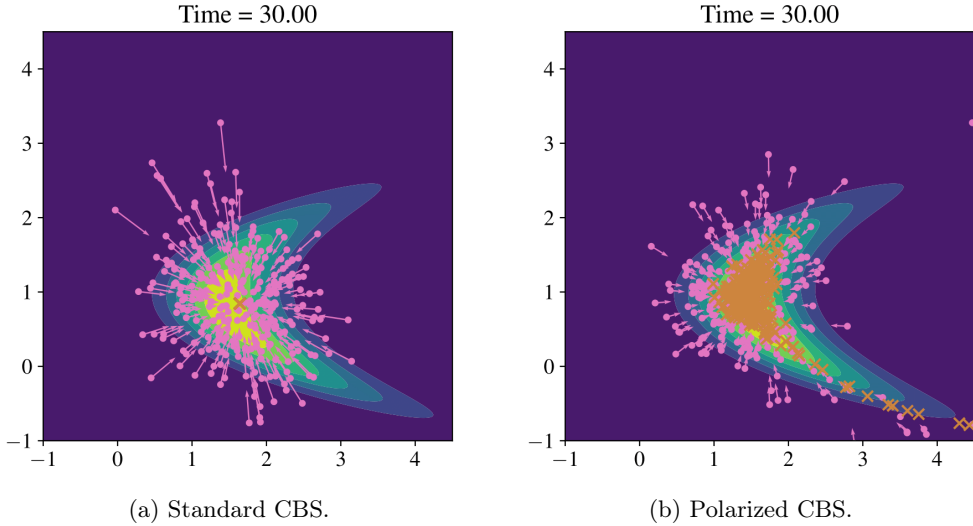


Figure 7: Standard and polarized CBS for sampling from a non-Gaussian distribution. The orange crosses mark the position of the weighted means.

4 Conclusion and Outlook

In this article we presented a polarized version of consensus-based optimization and sampling dynamics for objectives with multiple global minima or modes. For this we localized the dynamics such that every particle is primarily influenced by close-by particles. We proved that in the case of sampling from a Gaussian distribution this does not introduce a bias. We also suggested a cluster-based version of our polarized dynamics which is computationally more efficient. Our extensive numerical experiments suggested a large potential of our method for detecting multiple global minima or modes, improving over standard consensus-based methods.

There is a lot of room for future work regarding well-definedness of the Fokker–Planck equation derived above, and stability and convergence of both the mean-field and particle system to consensus. For this, a suitable quantity being able to track convergence to polarized consensus needs to be chosen and its behaviour for $t \rightarrow \infty$ needs to be analyzed. Future work will also focus on further numerical improvements of our method, in particular, incorporating a batching strategy similar to the one from [6] to further improve performance in high-dimensional optimization. Finally, a long-term goal will be to find multimodal sampling methods which are provably consistent for multimodal and non-Gaussian distributions. Given that even gradient-free sampling from unimodal non-Gaussian distributions is still relatively poorly understood, with [22] being a promising approach, this will be a challenging task for future work.

Acknowledgement

Part of this work was also done while LB and TR were in residence at Institut Mittag-Leffler in Djursholm, Sweden during the semester on *Geometric Aspects of Nonlinear Partial Differential Equations* in 2022, supported by the Swedish Research Council under grant no. 2016-06596. LB also acknowledges funding by the Deutsche Forschungsgemeinschaft (DFG, German Research Foundation) under Germany’s Excellence Strategy - GZ 2047/1, Projekt-ID 390685813. PW acknowledges support from MATH+ project EF1-19: Machine Learning Enhanced Filtering Methods for Inverse Problems, funded by the Deutsche Forschungsgemeinschaft (DFG, German Research Foundation) under Germany’s Excellence Strategy – The Berlin Mathematics Research Center MATH+ (EXC-2046/1,

project ID: 390685689). TR acknowledges support by the German Ministry of Science and Technology (BMBF) under grant agreement No. 05M2020 (DELETEO) and was supported by the European Unions Horizon 2020 research and innovation programme under the Marie Skłodowska-Curie grant agreement No 777826 (NoMADS).

References

- [1] D. Ackley. *A Connectionist Machine for Genetic Hillclimbing*. The Springer International Series in Engineering and Computer Science. Springer US, 2012. ISBN: 9781461319979.
- [2] Martin Burger. “Network structured kinetic models of social interactions”. In: *Vietnam Journal of Mathematics* 49.3 (2021), pp. 937–956.
- [3] Martin Burger. “Kinetic equations for processes on co-evolving networks”. In: *Kinetic and Related Models* 15.2 (2022), pp. 187–212.
- [4] José A Carrillo, Young-Pil Choi, Claudia Totzeck, and Oliver Tse. “An analytical framework for consensus-based global optimization method”. In: *Mathematical Models and Methods in Applied Sciences* 28.06 (2018), pp. 1037–1066.
- [5] José A Carrillo, Franca Hoffmann, Andrew M Stuart, and Urbain Vaes. “Consensus-based sampling”. In: *Studies in Applied Mathematics* 148.3 (2022), pp. 1069–1140.
- [6] José A Carrillo, Shi Jin, Lei Li, and Yuhua Zhu. “A consensus-based global optimization method for high dimensional machine learning problems”. In: *ESAIM: Control, Optimisation and Calculus of Variations* 27 (2021), S5.
- [7] José A Carrillo, Claudia Totzeck, and Urbain Vaes. “Consensus-based optimization and ensemble Kalman inversion for global optimization problems with constraints”. In: *arXiv preprint arXiv:2111.02970* (2021).
- [8] Andrew R Conn, Katya Scheinberg, and Luis N Vicente. *Introduction to derivative-free optimization*. SIAM, 2009.
- [9] Guillaume Deffuant, David Neau, Frederic Amblard, and Gérard Weisbuch. “Mixing beliefs among interacting agents”. In: *Advances in Complex Systems* 3.01n04 (2000), pp. 87–98.
- [10] Massimo Fornasier, Hui Huang, Lorenzo Pareschi, and Philippe Sünnen. “Consensus-based optimization on hypersurfaces: Well-posedness and mean-field limit”. In: *Mathematical Models and Methods in Applied Sciences* 30.14 (2020), pp. 2725–2751.
- [11] Massimo Fornasier, Timo Klock, and Konstantin Riedl. “Consensus-based optimization methods converge globally in mean-field law”. In: *arXiv preprint arXiv:2103.15130* (2021).
- [12] Massimo Fornasier, Lorenzo Pareschi, Hui Huang, and Philippe Sünnen. “Consensus-Based Optimization on the Sphere: Convergence to Global Minimizers and Machine Learning.” In: *J. Mach. Learn. Res.* 22.237 (2021), pp. 1–55.
- [13] Santo Fortunato, Vito Latora, Alessandro Pluchino, and Andrea Rapisarda. “Vector opinion dynamics in a bounded confidence consensus model”. In: *International Journal of Modern Physics C* 16.10 (2005), pp. 1535–1551.
- [14] Javier Gómez-Serrano, Carl Graham, and Jean-Yves Le Boudec. “The bounded confidence model of opinion dynamics”. In: *Mathematical Models and Methods in Applied Sciences* 22.02 (2012), p. 1150007.
- [15] Seung-Yeal Ha, Shi Jin, and Doheon Kim. “Convergence of a first-order consensus-based global optimization algorithm”. In: *Mathematical Models and Methods in Applied Sciences* 30.12 (2020), pp. 2417–2444.
- [16] Rainer Hegselmann and Ulrich Krause. “Opinion dynamics and bounded confidence models, analysis, and simulation”. In: *Journal of artificial societies and social simulation* 5.3 (2002).

- [17] J. Kennedy and R. Eberhart. “Particle swarm optimization”. In: *Proceedings of ICNN'95 - International Conference on Neural Networks*. Vol. 4. 1995, pp. 1942–1948.
- [18] Kaare Brandt Petersen, Michael Syskind Pedersen, et al. “The matrix cookbook”. In: *Technical University of Denmark* 7.15 (2008), p. 510.
- [19] René Pinnau, Claudia Totzeck, Oliver Tse, and Stephan Martin. “A consensus-based model for global optimization and its mean-field limit”. In: *Mathematical Models and Methods in Applied Sciences* 27.01 (2017), pp. 183–204.
- [20] Leonard Andreevič Rastrigin. “Systems of extremal control”. In: *Nauka* (1974).
- [21] Craig W Reynolds. “Flocks, herds and schools: A distributed behavioral model”. In: *Proceedings of the 14th annual conference on Computer graphics and interactive techniques*. 1987, pp. 25–34.
- [22] Claudia Schillings, Claudia Totzeck, and Philipp Wacker. “Ensemble-based gradient inference for particle methods in optimization and sampling”. In: *arXiv preprint arXiv:2209.15420* (2022).
- [23] Claudia Totzeck. “Trends in consensus-based optimization”. In: *Active Particles, Volume 3*. Springer, 2022, pp. 201–226.
- [24] Claudia Totzeck and Marie-Therese Wolfram. “Consensus-based global optimization with personal best”. In: *Mathematical Biosciences and Engineering* 17.5 (2020), pp. 6026–6044. ISSN: 1551-0018.